# Analysis and Design of the LLC LED Driver Based on State-Space Representation Direct Time-Domain Solution

Maikel F. Menke, *Student Member, IEEE*, João P. Duranti, Leandro Roggia, Fábio E. Bisogno, Rodrigo V. Tambara, and Álysson R. Seidel, *Member, IEEE*

***Abstract*—The LLC resonant converter has been widely used in switched power supply covering several kinds of applications. Although it has been the focus of numerous analysis, their general time-domain (TD) solution is not completely enclosed due to its complexity given by the multiple resonance nature and its variable structure behavior. Consequently, the LLC converter design is also impaired by the lack of an enclosed TD solution. To overcome these issues, this article systematically presents a highly accurate TD solution of the LLC converter supplying a light-emitting diode (LED) load, which is obtained from the state-space representation direct TD solution. Dissimilar to preceding analyses, all the converter states are considered and no current and voltage sinusoidal or average value approximations are taken. Finally, supported by the TD analysis, a new LLC LED driver design procedure is introduced, which is oriented by weighted-average-efficiency concept and constraints that ensure zero voltage switching, enough power gain, and practical switching frequency range over a wide operating window. Experimental results show the feasibility of the proposed design procedure as well as the accurate TD behavior prediction of the LLC converter supplying an LED load. This article is accompanied by active content that exemplifies the proposed TD solution and design procedure.**

***Index Terms*—Light-emitting diode (LED) driver, LLC resonant converter, state-space representation, time-domain (TD) analysis, wide operating range.**

## I. Introduction

NOWADAYS, the development of any new power supply pursues a system with high efficiency, high power density, and high reliability among several other characteristics. In this way, different proposals are found in the literature, being a trend in the employment of resonant-based converters, which have recognized advantages over its pulsewidth modulated counterparts when looking for a system with high efficiency and high power density. Thereby, resonant converters are becoming increasingly popular in industrial applications [1], and they consequently become the focus of current researches that deal with providing their enhanced analysis and design procedures.

Among resonant tank topologies, the LLC configuration has drawn considerable attention due to its capability to reach a wide operating range with high efficiency, together with the low level of electromagnetic interference emission, and its ability to achieve high power density [2]. Thus, it is widely used in different applications, such as in battery chargers [3], light-emitting diode (LED) drivers [4]–[6], and photovoltaic converters [7].

Regarding resonant converter analysis, the fundamental harmonic approximation (FHA) has become the standard method due to its simplicity, seeing that the system is originally nonlinear. Throughout the FHA analysis, all the voltage and current in the resonant circuit are assumed to be sinusoidal, and the output rectifier in dc/dc applications is modeled as an equivalent resistance, which allows to employ the classic ac analysis techniques [6], [8]. However, presuming the use of the LLC converter subjected to a wide operating range employing pulse frequency modulation (PFM), as the switching frequency ($f_S$) moves away from the main resonance ($f_o$), the FHA method becomes less accurate [1], [2], [9], [10]. Last but not least, due to the multiresonance behavior of the LLC, many details of the circuit operation in the time-domain (TD) will be lost in the FHA analysis [9], which are critical to define and evaluate the converter losses and obtain further insights of the converter behavior. In this way, to overcome these issues, a current effort in dealing with the dc/dc LLC resonant converter TD analysis is noted in the literature.

Analyzing the literature that deals with LLC converter steady-state TD analysis, several studies have been originated from the methodology proposed in [11]. These studies [1]–[3], [9]–[14], which follow the same backbone when considering the LLC TD solution, summarize the state-of-the-art technology, where the following common practices are noted.

1) All the LLC resonant stages are presented ($P$, $N$, and $O$), and for each stage, the differential equations that rule the evolution of a partial number of the system state variables are presented and solved.

Manuscript received August 4, 2019; revised November 18, 2019 and February 19, 2020; accepted May 6, 2020. Date of publication May 19, 2020; date of current version July 31, 2020. This work was supported in part by the Brazilian government through Coordenacão de Aperfeiçoamento de Pessoal de Nível Superior—Brasil (CAPES/PROEX)—Finance Code 001, PRPGP/UFSM, INCT-GD, CAPES proc. 23038.000776/2017-54, CNPq proc. 313338/2018-3, 409632/2016-3, and 465640/2014-1, and in part by FAPERGS proc. 17/2551-0000517-1. Recommended for publication by Associate Editor S. Kapat. *(Corresponding author: Maikel F. Menke.)*

The authors are with the Universidade Federal de Santa Maria, Santa Maria 97105-900, Brazil (e-mail: maikelmenke@gmail.com; joaopauloduranti@gmail.com; roggia@gmail.com; fbisogno@gepoc.ufsm.br; rodvarella10@gmail.com; seidel@ctism.ufsm.br).

This article has supplementary downloadable material available at http://ieeexplore.ieee.org, provided by the authors.

Color versions of one or more of the figures in this article are available online at https://ieeexplore.ieee.org.

Digital Object Identifier 10.1109/TPEL.2020.2995942

2) The different operation modes of the converter are analyzed with the respective main waveforms. An operation mode is defined as a single sequence of the different resonant stages.

3) For each mode, the constraint conditions that define the mode are presented.

4) After these sections, each article follows with its own focus, usually proposing a new design procedure.

Alternatively, there are other TD solution procedures proposed in the literature which are based on different approaches. For instance, Laplace-based theorem is proposed in [15] to obtain closed-form expressions for series resonant converter waveform. The cyclic-averaging technique for rapid resonant converter analysis is proposed in [16].

Nevertheless, considering the analysis derived from [11], even that quite accurate results are obtained in predicting the dc/dc LLC converter behavior in the TD, and there are common approximations that do not allow a general and accurate solution. The main approximations that simplify the analysis but avoid further insights of the converter are the following.

1) Converter output voltage is considered as a constant voltage source ($V_O$), which does not allow to enhance the output filter design and evaluate the output voltage and current ripple.

2) Voltage and current analysis in all the converter elements is avoided, being analyzed only a partial number of the system state variables.

3) The operation of the LLC converter is given for a 50% duty cycle with PFM.

4) All elements are considered ideal.

5) Load is treated as purely resistive.

Therefore, in order to overcome most of these shortcomings, in this article, a new TD solution procedure for the LLC LED driver converter is proposed. This procedure is based on the system state-space representation direct TD solution, where we have the following: 1) all the state variables of the converter are considered; 2) the output voltage is defined as the output filter capacitor voltage; and 3) LED load is examined as a piecewise linear (PWL) circuit. In this way, since a reduced number of approximations are made, it can be stated that the state-space general TD solution yields in highly accurate results. However, due to their complexity, its use in power electronics converters is usually set aside. Nevertheless, as it will be shown, employing the systematic procedure proposed to obtain the converter TD solution, the complexity will be diminished and all the efforts will be redirected to a numerical computational software. Finally, employing the proposed TD analysis procedure of the LLC LED driver, a new design procedure is introduced. Since it is usual in artificial lighting applications, the converter will be submitted to the different input voltages and load conditions. So, to contemplate this universe of operating points, the proposed design procedure is orientated by the weighted-average-efficiency concept. Besides, further constraints are assessed in order to ensure zero voltage switching (ZVS), enough power gain, and practical switching frequency range over the wide operating window. In this way, beyond a high performance LLC LED driver design, the proposed design procedure allows to predict with improved accuracy the performance of the converter due to the enhanced accuracy obtained, analyzing the LLC in the TD.

Hence, involved by the potentialities of the state-space representation and its accurate TD solution, the main contributions of this article are highlighted as follows: 1) proposal of a general and exact steady-state TD solution of the LLC resonant converter LED driver based on the system state-space equations representation; and 2) new design procedure for the LLC LED driver converter derived from the proposed TD solution, which ensures ZVS, enough power gain, and practical switching frequency range over a wide operating window.

The rest article is organized as follows. Section II presents the generic TD solution of a variable structure system represented in the state-space. Section III presents the resonant stages of the dc/dc LLC LED driver converter and the overview of its operating modes. In the sequence, Section IV presents the general exact TD solution of the LLC LED driver converter. Section V presents the proposed LLC converter design methodology, which is employed to design an LED driver in Section VI. In order to validate the proposed TD solution, derived analysis, and design procedure, experimental results are shown in Section VII. The main conclusion of this article is summarized in Section VIII.

## II. Basis of the Proposed TD Solution Procedure

A continuous-time (CT) linear time-invariant (LTI) system representation in state-space equations is given by the following equations [17], [18]:

$$\dot{\mathbf{x}}(t) = \mathbf{A}\mathbf{x}(t) + \mathbf{B}\mathbf{u}(t) \tag{1a}$$

$$\mathbf{y}(t) = \mathbf{C}\mathbf{x}(t) + \mathbf{D}\mathbf{u}(t) \tag{1b}$$

where $\mathbf{x}(t)$ is the state vector, $\mathbf{u}(t)$ is the input of the system, and $\mathbf{A}$, $\mathbf{B}$, $\mathbf{C}$, and $\mathbf{D}$ are constant matrices. Considering a switching cycle of any switched converter, for each controlled or uncontrolled switch state, a different equivalent structure is obtained, which characterizes a nonlinear system. On the other hand, since each equivalent structure of the system can be analyzed by a CT LTI system, the converter operation over a switching cycle can be modeled as a variable structure system, also named as a PWL system.

### A. Time-Domain Solution of a PWL System

Fig. 1 shows the evolution of a single state variable $x_i(t)$ over a switching cycle $T_S$ for a characterized PWL system. Each step in Fig. 1 corresponds to a CT LTI system. During the proposed analysis, $t_0$ is considered the origin time 0, which is in phase with the switches control signal. The time $t_{Z1}$ corresponds to the transition time between Step 1 (S1) and Step 2 (S2), $t_{Z2}$ corresponds to the transition time between S2 and Step 3 (S3), and so on. For the case shown in Fig. 1, the switching cycle is composed of six stages; thus, $t_{Z6} = T_S$.

Considering a PWL system in the state-space representation, we are interested to find out the solution for the state-vector $\mathbf{x}(t)$ excited by an input $\mathbf{u}(t)$ and initial state $\mathbf{x}(t_0)$ for $t_0$. However, in power electronics converters under steady-state operation, the initial state-vector $\mathbf{x}(t_0)$ usually defines inductor current and capacitor voltage values at the beginning of each switching

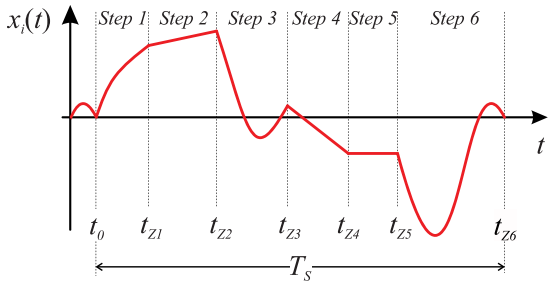


Fig. 1. Generic state-variable waveform in a variable structure system.

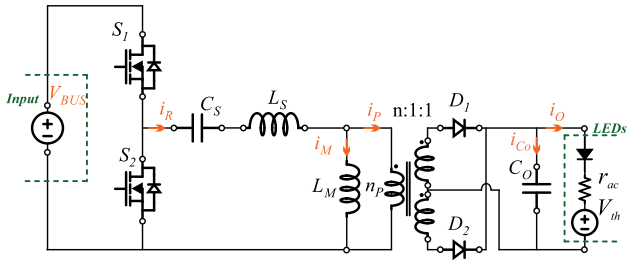


Fig. 2. DC/DC LLC resonant converter schematic diagram for an LED driver.

cycle, which are unknown values. Besides, taking into account the resonant converters' natural behavior, some transition times arise from indirectly controlled events; thus, they also become unknown variables. In this way, the problem is extended to find indirectly controlled transition times ($t_{ZN}$), state-vector $\mathbf{x}(t)$, and the initial state-vector $\mathbf{x}(t_0)$ excited by the input $\mathbf{u}(t)$.

The general equation that governs the state-vector variable evolution during a specific step, Step $N$ (SN), is given by (2) shown at the bottom of this page. Throughout SN, the state-vector values evolve from their initial condition $\mathbf{x}_{S(N-1)}(t_{Z(N-1)})$ up to its convergence value given by the state-vector value at the transition time $t_{ZN}$ that characterizes the end of the current Step $N$ and the beginning of the next step $N+1$. This convergence value $\mathbf{x}_{SN}(t_{ZN})$ is given by (3), shown at the bottom of this page. From (2) and (3), $\mathbf{x}_{S(N-1)}(t_{Z(N-1)})$ defines the state-vector initial value at Step $N$, which is given by the state-vector values at the end of step $N-1$. Since $\mathbf{x}_{S(N-1)}(t_{Z(N-1)})$ takes into account the initial state value at time 0 and the state variables evolve overall steps before $N$, its general expression is given by (4), shown at the bottom of this page. Here, $\mathbf{\Psi h_{SN}}(t_{ZN})$ and $\mathbf{\Psi p_{SN}}(t_{ZN})$ are given in the following two equations, respectively:

$$\mathbf{\Psi h_{SN}}(t_{ZN}) = e^{\mathbf{A_{SN}}(t_{ZN}-t_{Z(N-1)})} \tag{5}$$

$$\mathbf{\Psi p_{SN}}(t_{ZN}) = \int_0^{t_{ZN}-t_{Z(N-1)}} e^{-\mathbf{A_{SN}}(\zeta)}\mathbf{B_{SN}}\mathbf{u}(\zeta)d\zeta. \tag{6}$$

As can be seen in the presented analysis up to this point, for each step SN, there are two main equations. The first one governs the evolution of the state-vector variables taking into account the initial condition at this step as well as the input excitation. The second equation gives the exact value of the state vector at the transition time that characterizes the end of the associated step. Thus, to obtain the TD solution of a PWL system, it becomes necessary to compute (3) and (4). However, considering that the input $\mathbf{u}(t)$ is constant over $T_S$, the matrix exponential integral computation can be computed by the following equation for non-singular $\mathbf{A}$, which avoids a numerical integration diminishing the required computational effort

$$\int_0^t e^{\mathbf{A}t}\mathbf{B}\mathbf{u}(t)dt = \mathbf{A}^{-1}(e^{\mathbf{A}t} - \mathbf{I})\mathbf{B}\mathbf{u}. \tag{7}$$

## III. DC/DC LLC Converter Stage Analysis And Operation Mode Overview

Fig. 2 shows the schematic circuit diagram of an LED driver based on the dc/dc LLC resonant converter. As a function of the resonant tank elements ($L_S$, $C_S$, $L_M$, $n$), input bus voltage ($V_{\text{BUS}}$), half-bridge (HB) switching frequency ($f_S$), and load conditions ($r_{\text{ac}}$, $V_{\text{th}}$), the LLC LED driver converter can operate with multiple resonant stages within one switching cycle ($T_S$). Analyzing one switching cycle of the converter in the steady-state operation, six possible resonant stages are identified, which are classified as a function of the transformer magnetizing inductance ($L_M$), voltage ($v_{Lm}$), and HB switches ($S_1$, $S_2$) state (ON or OFF).

As PFM with a fixed 50% duty cycle is usually employed to regulate LLC converter output voltage and/or current, the resonant tank waveforms are symmetrical to the half switching cycle ($T_S/2$) [9]. Therefore, it is possible to simplify the LLC examination focusing the analysis in the resonant stages that occur during the first half switching cycle, defined when $S_1$ is ON and $S_2$ is OFF.

Fig. 3 shows the LLC LED driver equivalent circuit for each possible resonant stage throughout the first half switching cycle. The resonant stage characterized by $L_M$ positive clamped $v_{Lm}(t) = nv_{Co}(t)$ is named Stage P, where $v_{Co}(t)$ is the output capacitor ($C_O$) voltage and $n$ the transformer turns ratio. In the same way, for $L_M$ negative clamped $v_{Lm}(t) = -nv_{Co}(t)$, the stage is named N. Finally, the stage where $v_{Lm}(t) < nv_{Co}(t)$ is named Stage O. Unlike all the aforementioned works that deal

$$\mathbf{x_{SN}}(t) = e^{\mathbf{A_{SN}}(t-t_{Z(N-1)})}\mathbf{x_{S(N-1)}}(t_{Z(N-1)}) + \int_{t_{Z(N-1)}}^{t} e^{\mathbf{A_{SN}}(t-\tau)}\mathbf{B_{SN}}\mathbf{u}(\tau)d\tau \tag{2}$$

$$\mathbf{x_{SN}}(t_{ZN}) = \mathbf{\Psi h_{SN}}(t_{ZN})\mathbf{x_{S(N-1)}}(t_{Z(N-1)}) + \mathbf{\Psi h_{SN}}(t_{ZN})\mathbf{\Psi p_{SN}}(t_{ZN}) \tag{3}$$

$$\mathbf{x_{S(N-1)}}(t_{Z(N-1)}) = \left[\prod_{i=N}^{2}\mathbf{\Psi h_{S}}_{(i-1)}\left(t_{Z(i-1)}\right)\right]\mathbf{x_{S1}}(t_0) + \sum_{k=1}^{N-1}\left[\prod_{i=N}^{k+1}\mathbf{\Psi h_{S}}_{(i-1)}\left(t_{Z(i-1)}\right)\right]\mathbf{\Psi p_{Sk}}(t_{Zk}) \tag{4}$$

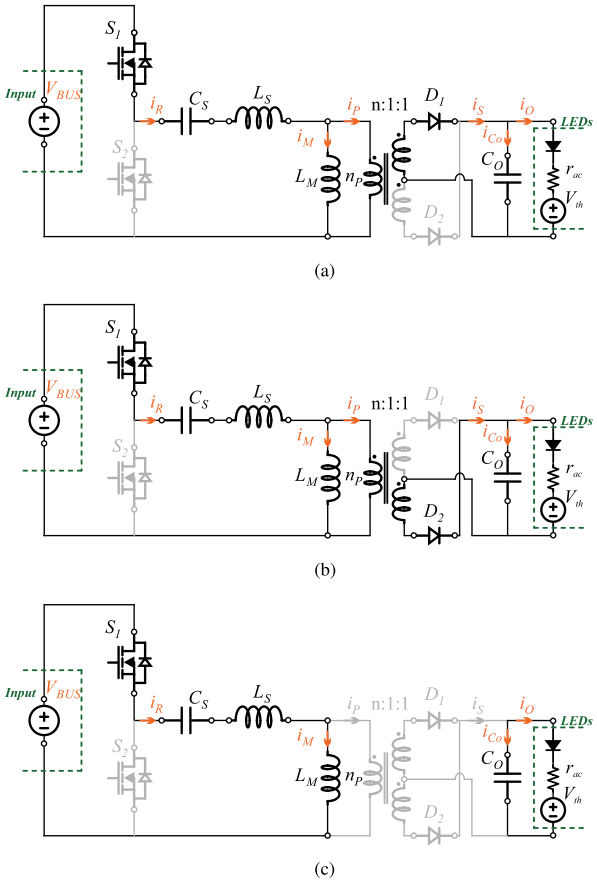


Fig. 3. DC/DC LLC resonant converter stages equivalent circuit for S1 ON and S2 OFF. (a) Stage P. (b) Stage N. (c) Stage O.

with the LLC TD solution, it should be noted that the output voltage is not approximated by its average value $V_O$. In order to maintain the objectivity, further description of the voltage and current behavior in the different resonant stages is here omitted since it has been presented in [1]–[3] and [9]–[14].

Dissimilar to previously reported studies, where the state-space representation is avoided, this article, for the first time in the literature, proposes to analyze the dc/dc LLC LED driver resonant converter with the direct TD solution of the state-space equation, which will result in the general and exact TD behavior prediction of the converter, independently of its parameters and operating conditions.

### A. State-Space Equations

Applying Kirchhoff's voltage and current laws on the equivalent circuit of Stage P shown in Fig. 3, the differential equations that rule the evolution of each state variable are obtained. For convenience, the state-vector variables considered in this article are shown in (8). The state variables differential equations for Stage P are given by (9)

$$\mathbf{x}(t) = \begin{bmatrix} i_R(t) & v_{Cs}(t) & i_M(t) & v_{Co}(t) \end{bmatrix}^T. \tag{8}$$

Considering the state variables $\mathbf{x}(t)$ and state differential equations, each resonant stage can be represented by the equivalent state-space equation, defined by (1). For Stage P, the constant matrices are named as $\mathbf{A_P}$ and $\mathbf{B_P}$ and shown in (10) and (11), respectively. Besides, the input signals are given by (12), which are time-independent variables over $T_S$.

On the other hand, applying Kirchhoff's voltage and current laws on the equivalent circuit of Stage N shown in Fig. 3, the system state-space equations are determined, being the matrices $\mathbf{A_N}$ and $\mathbf{B_N}$ shown in (13) and (14), respectively. Similarly, considering the equivalent circuit of Stage O, the matrices $\mathbf{A_O}$ and $\mathbf{B_O}$ are shown in (15) and (16), respectively.

The analysis presented upon this point considers the LED PWL circuit. Focusing on this equivalent circuit, it is easy to see that a more functional solution will be obtained since it can be easily adapted to resistive loads doing $V_{\text{th}} = 0$ and $r_{\text{ac}} = R_L$ or even employed to design LLC-based battery charger, where load can be modeled by the same PWL circuit

$$\frac{di_R(t)}{dt} = \frac{V_{\text{BUS}}}{L_S} - \frac{v_{C_S}(t)}{L_S} - \frac{nv_{Co}(t)}{L_S} \tag{9a}$$

$$\frac{dv_{Cs}(t)}{dt} = \frac{i_R(t)}{C_S} \tag{9b}$$

$$\frac{di_M(t)}{dt} = \frac{nv_{Co}(t)}{L_M} \tag{9c}$$

$$\frac{dv_{Co}(t)}{dt} = \frac{ni_R(t)}{C_O} - \frac{ni_M(t)}{C_O} - \frac{v_{Co}(t)}{r_{\text{ac}}C_O} + \frac{V_{\text{th}}}{r_{\text{ac}}C_O} \tag{9d}$$

$$\mathbf{A_P} = \begin{bmatrix} 0 & -\frac{1}{L_S} & 0 & -\frac{n}{L_S} \\ \frac{1}{C_S} & 0 & 0 & 0 \\ 0 & 0 & 0 & \frac{n}{L_M} \\ \frac{n}{C_O} & 0 & -\frac{n}{C_O} & -\frac{1}{r_{\text{ac}}C_O} \end{bmatrix} \tag{10}$$

$$\mathbf{B_P} = \begin{bmatrix} \frac{1}{L_S} & 0 & 0 & 0 \\ 0 & 0 & 0 & \frac{1}{r_{\text{ac}}C_O} \end{bmatrix}^T \tag{11}$$

$$\mathbf{u}(t) = \begin{bmatrix} V_{\text{BUS}} & V_{\text{th}} \end{bmatrix}^T \tag{12}$$

$$\mathbf{A_N} = \begin{bmatrix} 0 & -\frac{1}{L_S} & 0 & \frac{n}{L_S} \\ \frac{1}{C_S} & 0 & 0 & 0 \\ 0 & 0 & 0 & -\frac{n}{L_M} \\ -\frac{n}{C_O} & 0 & \frac{n}{C_O} & -\frac{1}{r_{\text{ac}}C_O} \end{bmatrix} \tag{13}$$

$$\mathbf{B_N} = \begin{bmatrix} \frac{1}{L_S} & 0 & 0 & 0 \\ 0 & 0 & 0 & \frac{1}{r_{\text{ac}}C_O} \end{bmatrix}^T \tag{14}$$

$$\mathbf{A_O} = \begin{bmatrix} 0 & \frac{-1}{L_S+L_M} & 0 & 0 \\ \frac{1}{C_S} & 0 & 0 & 0 \\ 0 & \frac{-1}{L_S+L_M} & 0 & 0 \\ 0 & 0 & 0 & \frac{-1}{r_{\text{ac}}C_O} \end{bmatrix} \tag{15}$$

$$\mathbf{B_O} = \begin{bmatrix} \frac{1}{L_S+L_M} & 0 & \frac{1}{L_S+L_M} & 0 \\ 0 & 0 & 0 & \frac{1}{r_{\text{ac}}C_O} \end{bmatrix}^T. \tag{16}$$

### B. DC/DC LLC Converter Operation Mode Overview

Different successive combinations of the resonant stages (P, N, and O) will determine the converter operation mode. For instance, PO mode indicates that in the first step, the resonant tank operates at Stage P and then at the transition time $t_{Z1}$

enters Stage O (second step), which is finished at $t_{Z2} = T_S/2$. Due to the aforementioned symmetrical behavior of a resonant converter with a constant 50% duty-cycle operation, only the stages in the first half-cycle are used to define and analyze each operation mode of the LLC converter.

In general, there are six main operation modes: PO, PON, PN, NP, NOP, and OPO also previously recognized in [9], [10], [11], and [13]. Fig. 4 shows the dc/dc LLC resonant converter main waveforms for the main different operation modes, where $t_0$ refers to the time 0 which is in phase with the switch $S_1$ gate signal $v_{GS1}$. As it can be seen in Fig. 4, each mode has its own voltage and current behavior and particular condition which define the sequence of the stages. In Fig. 4, $i_R$ corresponds to the resonant current, $i_M$ and $v_{Lm}$ are the transformer magnetizing inductance current and voltage, respectively, $v_{Cs}$ is the series capacitor $C_S$ voltage, and $i_{D1}$ and $i_{D2}$ correspond to the output rectifier current. The incidence of each mode for a given designed converter is a function of the $f_S$, load condition, and $V_{\text{BUS}}$, besides the own resonant tank parameters $C_S$, $L_S$, $L_M$, and $n$. Thus, all these variables have to be taken into account under the steady-state TD solution and analysis of the converter, which will be presented in the next section.

## IV. LLC LED Driver TD Solution

This section describes the procedure to obtain the steady-state TD solution of the dc/dc LLC LED driver employing the state-space representation direct TD solution. However, in order to further elucidate the proposed TD solution procedure, the active content of this article presents a sample of the code implemented in Wolfram MATHEMATICA to solve the LLC LED driver under PO mode operation. In addition, since the converter operation mode has to be known in order to apply the correct constraints and use the related constant matrices, and so obtain the correct TD solution, an operation mode solver algorithm is also proposed to accurately predict the converter operation mode.

### A. Steady-State TD Solution Procedure

In steady-state operation, the transition times $t_{ZN}$ together with the $\mathbf{x}(t_0)$ are the unknown variables to be initially determined. With these variables defined and known $\mathbf{u}(t)$ of the converter, taking into account the equations that govern the evolution of $\mathbf{x}(t)$ over each step in the TD, the problem around the state-space representation TD solution for the LLC LED driver is totally solved.

Assuming first that the operation modes (PO, PON, PN, NP, NOP, and OPO) and all the parameters $C_S$, $L_S$, $L_M$, $n$, $C_O$, $V_{\text{BUS}}$, $f_S$, $r_{\text{ac}}$, and $V_{\text{th}}$ are known, the procedure to obtain the TD steady-state solution of the LLC resonant converter is described step by step, as follows. It should be noted that average output current ($I_O$) and voltage ($V_O$) are not previously defined since they are outcomes depending on the system parameters and input signals.

*1) Set Up the System of Equations to be Numerically Solved:* To determine $t_{ZN}$ and $\mathbf{x}(t_0)$, the equations that defined the state-vector value at the transition times ($\mathbf{x}(t_{ZN})$) are used,

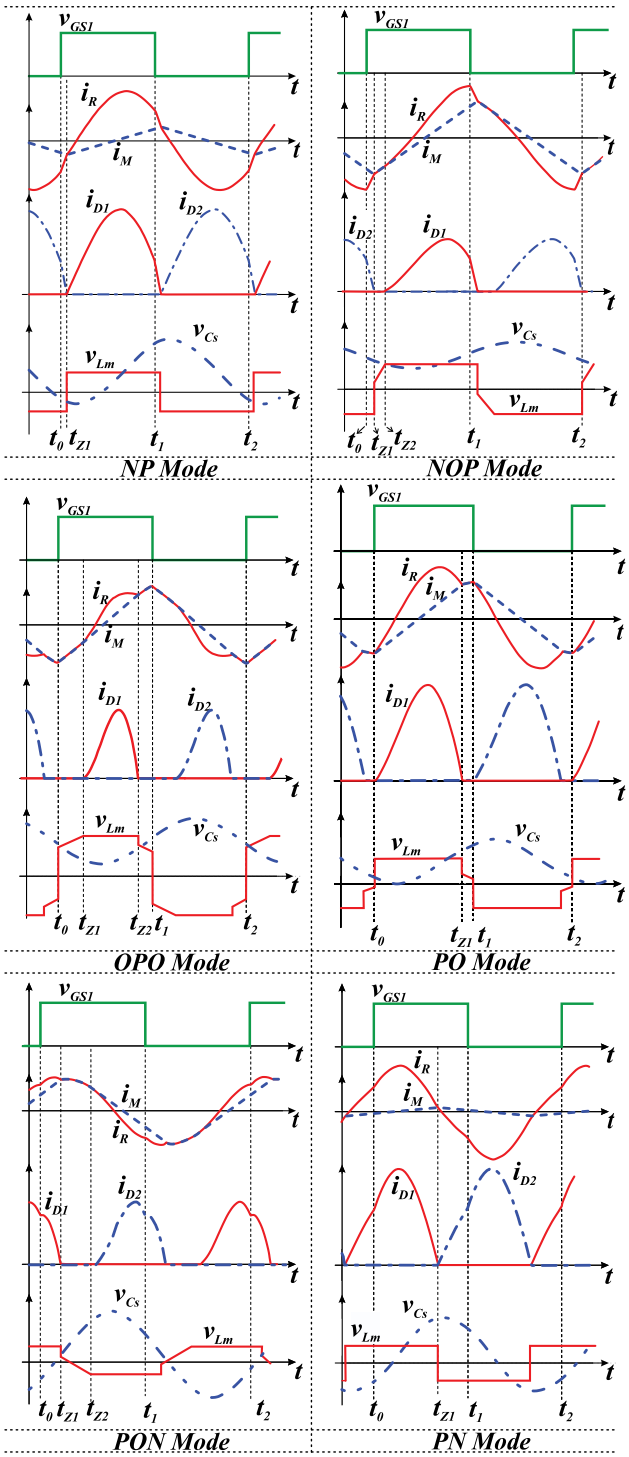


Fig. 4. Typical dc/dc LLC operation mode main waveforms.

where a system of equations is established and numerically solved to find the unknown variables. Therefore, considering the symmetrical behavior of the LLC converter, it is possible to see in Fig. 4 that the state-vector values at $t_1$, being $t_1 = T_S/2$, have a close relationship with their initial condition at $t_0$. The initial state-vector $\mathbf{x}(t_0)$ is given by (17), where its relationship with the state-vector values at $t_1$ is defined by (18) for all operating

modes. Accepting this relationship, it is possible to see (18) as a system of equations, where the left side of (18a)–(18d) is computed by (3)

$$\mathbf{x}(t_0) = \begin{bmatrix} I_{R0} & V_{CS0} & I_{M0} & V_{CO0} \end{bmatrix}^T \tag{17}$$

$$i_R(t_1) = -I_{R0} \tag{18a}$$

$$v_{Cs}(t_1) = V_{\text{BUS}} - V_{CS0} \tag{18b}$$

$$i_M(t_1) = -I_{M0} \tag{18c}$$

$$v_{Co}(t_1) = V_{CO0}. \tag{18d}$$

Nevertheless, considering, for example, the PO mode, there are five unknown variables ($I_{R0}$, $V_{CS0}$, $I_{M0}$, $V_{CO0}$, and $t_{Z1}$); however, only four equations are presented in (18a)–(18d). Thus, to be able to solve this system of equations, a fifth equation has to be defined. So, analyzing the PO mode main waveforms shown in Fig. 4, it can be seen that $i_R$ at $t_{Z1}$ is equal to the $i_M$, from where the missing equation is defined, given by the following equation:

$$i_R(t_{Z1}) = i_M(t_{Z1}). \tag{19}$$

Following this same analysis procedure, the unknown variables and the system equations that have to be solved for each LLC LED driver converter operation mode are presented in Table I. Defining the system of equations to be solved, any mathematical software with embedded algorithms to solve a nonlinear system of equations can be used. In addition, based on the analysis being carried out, some variables may become known, which shrink the systems of equations that need to be solved.

*2) Steady-State Time-Domain Solution and Analysis:* Once knowing $t_{ZN}$ and $\mathbf{x}(t_0)$ and employing (2) that governs the state variable evolution in each step, it is possible to define the system state variables in the TD by a piecewise equation. Considering a three-step operation mode, the following equation elucidates this approach:

$$\mathbf{x}(t) = \begin{cases} \mathbf{x_{S1}}(t) & \text{if } t_0 < t \leq t_{Z1} \\ \mathbf{x_{S2}}(t) & \text{if } t_{Z1} < t \leq t_{Z2} \\ \mathbf{x_{S3}}(t) & \text{if }, t_{Z2} < t \leq t_{Z3} = T_S/2. \end{cases} \tag{20}$$

At this point, (20) could be employed to plot each state variable evolution in the TD, which could support further insights of the LLC converter. On the other hand, with these same equations, it is possible to investigate particular conditions, for instance, the turn-OFF current of the HB switches, which is not possible with the FHA approach and not completely covered in the literature that deals with the TD solution. Furthermore, with few calculations, the output average current and voltage levels can be defined, as well as rms currents in the resonant tank and so on, culminating in a general and complete LLC converter analysis.

TABLE I
UNKNOWN VARIABLES AND SYSTEM OF EQUATIONS FOR EACH OPERATION MODE OF THE LLC CONVERTER

| Mode | Variables | System to solve |
|---|---|---|
| NP | $I_{R0}$ | $i_R(t_{Z2}) = -I_{R0}$ |
| | $V_{CS0}$ | $v_{Cs}(t_{Z2}) = V_{BUS} - V_{CS0}$ |
| | $I_{M0}$ | $i_M(t_{Z2}) = -I_{M0}$ |
| | $V_{CO0}$ | $v_{Co}(t_{Z2}) = V_{CO0}$ |
| | $t_{Z1}$ | $i_R(t_{Z1}) = i_M(t_{Z1})$ |
| NOP | $I_{R0}$ | $i_R(t_{Z3}) = -I_{R0}$ |
| | $V_{CS0}$ | $v_{Cs}(t_{Z3}) = V_{BUS} - V_{CS0}$ |
| | $I_{M0}$ | $i_M(t_{Z3}) = -I_{M0}$ |
| | $V_{CO0}$ | $v_{Co}(t_{Z3}) = V_{CO0}$ |
| | $t_{Z1}$ | $i_R(t_{Z1}) = i_M(t_{Z1})$ |
| | $t_{Z2}$ | $\frac{L_M}{L_M+L_S}(V_{BUS} - v_{Cs}(t_{Z2})) = nv_{Co}(t_{Z2})$ |
| OPO | $I_{R0}$ | $i_R(t_{Z3}) = -I_{R0}$ |
| | $V_{CS0}$ | $v_{Cs}(t_{Z3}) = V_{BUS} - V_{CS0}$ |
| | $I_{M0}$ | $i_M(t_{Z3}) = -I_{M0}$ |
| | $V_{CO0}$ | $v_{Co}(t_{Z3}) = V_{CO0}$ |
| | $t_{Z1}$ | $i_R(t_{Z2}) = i_M(t_{Z2})$ |
| | $t_{Z2}$ | $\frac{L_M}{L_M+L_S}(V_{BUS} - v_{Cs}(t_{Z1})) = nv_{Co}(t_{Z1})$ |
| PO | $I_{R0}$ | $i_R(t_{Z2}) = -I_{R0}$ |
| | $V_{CS0}$ | $v_{Cs}(t_{Z2}) = V_{BUS} - V_{CS0}$ |
| | $I_{M0}$ | $i_M(t_{Z2}) = -I_{M0}$ |
| | $V_{CO0}$ | $v_{Co}(t_{Z2}) = V_{CO0}$ |
| | $t_{Z1}$ | $i_R(t_{Z1}) = i_M(t_{Z1})$ |
| PON | $I_{R0}$ | $i_R(t_{Z3}) = -I_{R0}$ |
| | $V_{CS0}$ | $v_{Cs}(t_{Z3}) = V_{BUS} - V_{CS0}$ |
| | $I_{M0}$ | $i_M(t_{Z3}) = -I_{M0}$ |
| | $V_{CO0}$ | $v_{Co}(t_{Z3}) = V_{CO0}$ |
| | $t_{Z1}$ | $i_R(t_{Z1}) = i_M(t_{Z1})$ |
| | $t_{Z2}$ | $\frac{L_M}{L_M+L_S}(V_{BUS} - v_{Cs}(t_{Z2})) = nv_{Co}(t_{Z2})$ |
| PN | $I_{R0}$ | $i_R(t_{Z2}) = -I_{R0}$ |
| | $V_{CS0}$ | $v_{Cs}(t_{Z2}) = V_{BUS} - V_{CS0}$ |
| | $I_{M0}$ | $i_M(t_{Z2}) = -I_{M0}$ |
| | $V_{CO0}$ | $v_{Co}(t_{Z2}) = V_{CO0}$ |
| | $t_{Z1}$ | $i_R(t_{Z1}) = i_M(t_{Z1})$ |

## B. Mode Solver

In the last section, the steady-state TD solution of the LLC LED driver converter was developed, assuming that the operation mode was known. However, to automatically determine the operation mode of the converter for given parameters, load condition, and input voltage, usually, an algorithm named mode solver is employed [1], [10]. Therefore, in order to disclose the converter operation mode, the state values at the transition times and specific constraints related to the magnetizing inductance voltage are assessed. Based on the developed converter TD solution, the proposed mode solver is shown in Fig. 5, where the solver can be easily adapted to identify the correct mode considering different unknown parameters. For instance, if $I_O$ and $V_O$ are given, the mode solver will define the required $f_S$ to achieve these values as well as determine the associated operation mode. On the other hand, if defined the $f_S$, the mode solver will find the correspondent operation mode and define the yielding $I_O$ and $V_O$.

With the LLC LED driver completely solved in the TD, the next section proposes a new design procedure, which relies on the analysis of the converter carried out in the TD.

# V. PROPOSED LLC CONVERTER DESIGN PROCEDURE

A well-designed dc/dc LLC LED driver converter presents ZVS operation and enough peak gain to keep the output (voltage

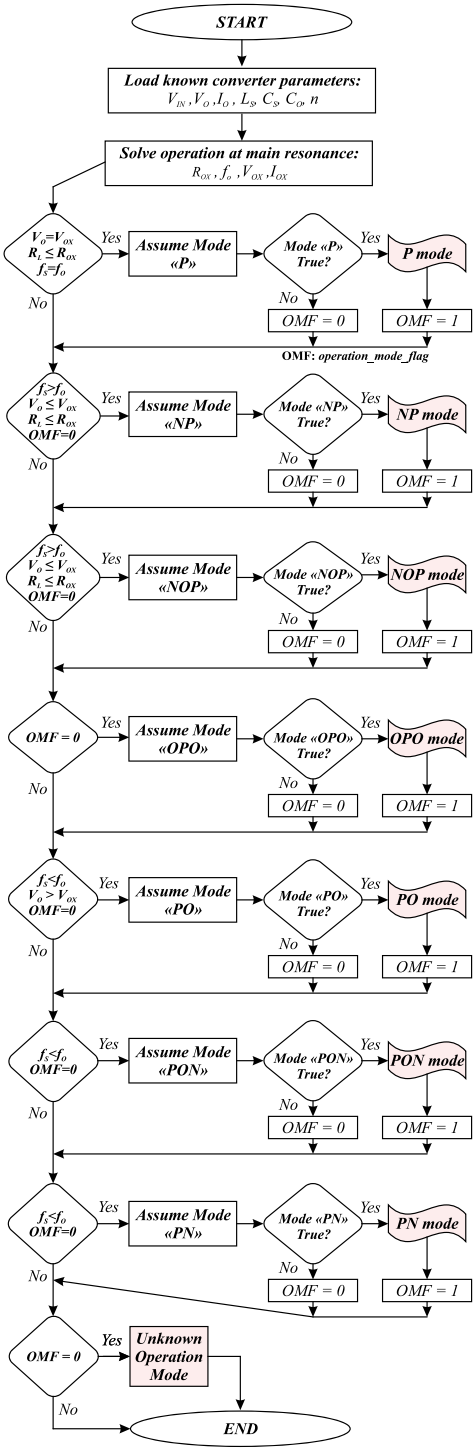


Fig. 5. DC/DC LLC resonant converter proposed mode solver.

and/or current) controlled over the whole operating window while maintaining good efficiency. In this way, usually voltage and current gain curves, as well as the maximum peak gain, are evaluated in design methodologies reported in the literature, where TD and FHA approaches have been used [2], [9]. However, due to FHA lack of accuracy, TD-based design procedures are preferable to design the LLC converter that has to operate over a wide range.

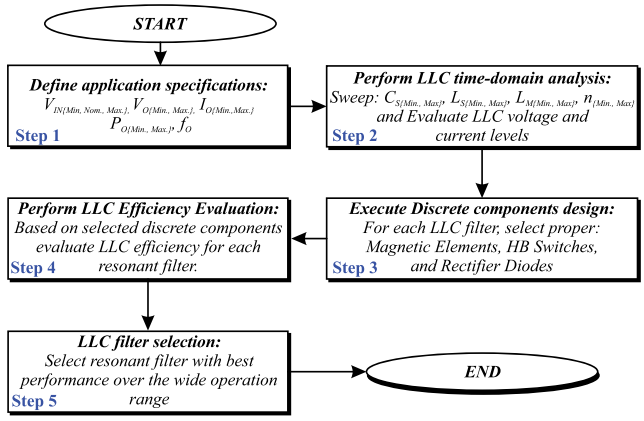


Fig. 6. Proposed LLC converter design procedure algorithm flowchart.

On the other hand, in order to improve the LLC converter performance, several design methodologies carefully assess the resonant component influence on the converter current levels, being selected the inductance and capacitance that result in lower resonant and switches current levels. However, these design approaches rely on the analysis carried out usually only for the nominal operating point or partially covering the whole operating window. In addition, converter power density and efficiency is seldom directly evaluated during the design stage.

To overcome these drawbacks, a new design procedure is proposed considering the wide operating range of the converter, where, instead of current and voltage levels, the estimated converter efficiency is employed to guide the inductance and capacitance values definition of the LLC converter. Nevertheless, to take into account the converter efficiency under different operating points, and not only at nominal condition, a figure of merit based on weighted average efficiency is employed, which considers in its definition the efficiency at different load conditions and operation cases that the converter will be submitted. Different operation cases are understood as the variation of input voltage and load configuration or the combination of both. In addition, to ensure ZVS, enough current gain, and feasible switching frequency range, the design procedure is supported by constraints that add these features to the designed converter. Besides, the power density of the converter is also assessed before culminating the design with the resonant tank parameter definitions. Last but not least, to outcome in a reliable designed converter, the proposed LLC state-space representation direct TD solution is employed, which guarantees that the converter behavior is considered with high accuracy, which does not occur if the FHA approach is employed.

Fig. 6 shows the proposed design procedure algorithm flowchart, where steps are described as follows.

### A. Step 1: Application Specifications

The design procedure starts by defining the parameters that delimit the LLC converter operating range for a given application. In this way, the input voltage $V_{\text{IN}} = V_{\text{BUS}}$, output voltage $V_O$, output current $I_O$, and output power $P_O$ range $\{\min, \max\}$ are defined. Furthermore, the main resonant frequency ($f_o$) of

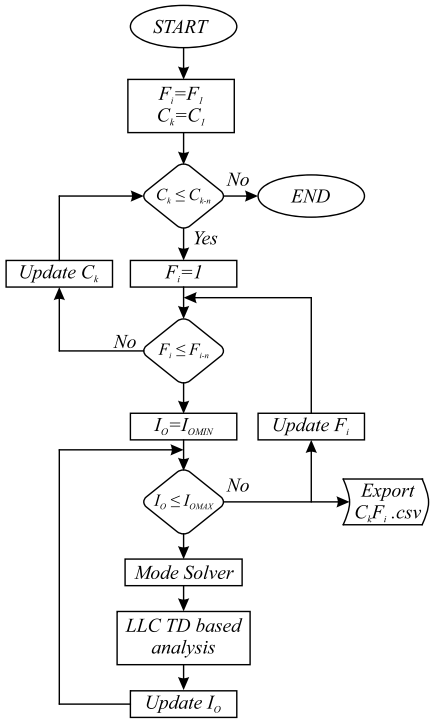


Fig. 7. LLC design procedure Step 2 flowchart.

the system has to be defined, which implies upon switching frequency region of the converter. In a general point of view, Step 1 consists of design input parameters knowledge.

### B. Step 2: LLC Time-Domain Analysis

To perform the LLC LED driver TD analysis, real filter elements have to be employed. Therefore, considering a set of resonant tank elements ($C_S$, $L_S$, $L_M$, $n$), the second step of the design procedure accurately analyzes each LLC filter from the set in the TD employing the proposed system state-space representation direct TD solution. To tackle this task, the algorithm sketched in Fig. 7 is implemented. In which, from the application specifications, the combinations of $V_{\text{IN}}$ and/or $V_O$ define different operation cases ($C_1$, $C_2$, ..., $C_{k-n}$), and the possible combinations among $L_S$, $C_S$, $n$, $L_M$ define different LLC filters ($F_1$, $F_2$, ..., $F_{i-n}$). Finally, for each case $C_k$, the same set of resonant tanks $F_i$ is evaluated in the TD considering load variation ($I_{O\text{MIN}} - I_{O\text{MAX}}$). Analyzing Fig. 7, it can be seen that for each filter, case, and load condition, the LLC mode solver is employed to predict the converter mode (PN, PON, PO, P, OPO, NOP, or NP). With the mode identified, current and voltage levels in the main elements of the LLC are calculated by employing the procedure presented in Section IV-A2.

Gathering the outcomes throughout load sweep for each filter $F_i$ and operating case $C_k$, an array of data is exported, which is used by the next design procedure step. To maintain clarity, each array carries in its variable name the information of the current case and filter evaluated. For example, $C_1F_1$ stands for "Case 1" and "Filter 1" and so on for all cases ($C_k$) and filters ($F_i$) analyzed. Each row of this array corresponds to a specific

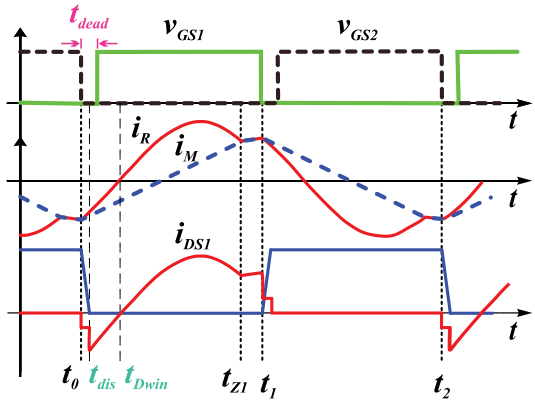


Fig. 8. DC/DC LLC converter main waveform to assess the true ZVS conditions.

output current $I_O$, and the columns bring the related $V_{\text{IN}}$, $V_O$, $f_S$, $C_S$, $L_S$, $L_M$, resonant rms ($i_{R.\text{rms}}$) and peak ($i_{R.pk}$) current, rms $C_S$ voltage ($v_{Cs.\text{rms}}$), HB switches rms ($i_{S1.\text{rms}}$), peak ($i_{S1.pk}$) and turn-OFF($i_{S1.\text{off}}$) current, secondary rms current ($i_{\text{Sec.rms}}$), rectifier average current ($i_{D1.\text{avg}}$), and resonant filter input current phase expressed in the TD as the HB duty-cycle window $t_{D\text{win}}$ (see Fig. 8).

From a macro point of view, this second step performs the TD analysis of several LLC filters sweeping over different loads and input voltages where, from this set of filters, the most suitable one, considering the imposed constraints and design requirements, will be selected at the end of the design procedure.

### C. Step 3: Discrete Components Design

The data generated by Step 2 are now employed to design the proper semiconductors and magnetic elements for each filter $F_i$. In this way, for each $F_i$ filter evaluated, the critical operation point is identified among all cases ($C_k$) that this filter would be submitted if employed. The critical operation point corresponds to the condition where the highest current and voltage levels are noted. In sequence, the critical operating point condition is employed to select the semiconductors and design the converter magnetic elements.

The procedure of designing especially the proper magnetic elements for each evaluated filter $F_i$ allows a fair comparison among them, which differs from the methodologies that first define the magnetic element size that will be employed and then design the resonant tank. It is worthy to mention that different magnetic element sizes have an impact on the converter losses and power density; therefore, the proper magnetic element selection for each filter besides a fair comparison could bring the converter to higher efficiency and power density.

With the identified critical operating condition for each filter $F_i$, the magnetic element (series resonant inductor and transformer) design is given following the next steps.

1) Based on the maximum rms current, the wires are designed.

2) Employing the well-known **AeAw** method, the minimum core size required is defined.

3) Selecting the core size, the number of turns for each coil is calculated.

4) Estimate the dc resistance of the coil based on wire parameters and number of turns.

In sequence, the HB switches and output rectifier diodes are easily selected based on the maximum stress noted for each filter.

### D. Step 4: LLC Power Losses and Efficiency Computation

At this point, the current and voltage levels for each $F_i$ operating overall $C_k$ with a variable load are known and available on the $C_kF_i$.csv file (Step 2 result) as well as the employed semiconductors and magnetic elements in each $F_i$ (Step 3 result), which allows the converter efficiency to be estimated (Step 4 duty). Hence, the converter power losses are calculated for each filter $F_i$ operating with a variable load under all $C_k$ considered. With the power losses calculated, the efficiency ($\eta$) is estimated by (21). LLC converter power losses are calculated based on the classic losses model, described with details in [1], [12], and [13]

$$\text{Efficiency} = \eta = \frac{\text{Output Power}}{\text{Power Losses} + \text{Output Power}}. \tag{21}$$

### E. Step 5: LLC Filter Selection

The final step of the proposed design procedure aims to select one LLC filter from the initial set of LLC filters $F_i$. Differing from the conventional approaches where the resonant tank elements are designed based only on the current levels, the proposed design relies on the efficiency curves and additional constraint evaluation that ensures a reliable design and does not deteriorate converter performance. As it will be seen, besides an improved performance, the merit of the proposed design relies also on the complete prediction of the converter performance, allowing the designer to take decisions in advance in order to address the design requirements.

*1) Peak Gain Evaluation:* The first step in the LLC filter selection will exclude from the possible solutions the $F_i$ that does not present enough peak gain to maintain the output controlled over the specified application operating range. This task is done by evaluating $C_kF_i$.csv for each filter and checking if the maximum output power is reached under extreme cases.

*2) Efficiency Evaluation:* Since the converter is submitted to a wide operating range considering input voltage as well as output voltage and current variation, a metric related to the average efficiency is proposed to compare different filter efficiency performances. In this way, for each LLC filter $F_i$ considering the operation at a specific output power ($P_j$), the average efficiency ($\langle\eta\rangle_{@P_j}$) is calculated among the assessed operating cases $C_k$, given by the following equation:

$$\langle\eta\rangle_{P_j} = \frac{1}{k}\sum_{C_1}^{C_k}\eta_{CkPj}. \tag{22}$$

Considering that the converter operates with different loads, the average efficiency calculation in (22) does not outcome in a single efficiency performance index for each filter. Therefore, in order to rank the LLC filters from the efficiency performance point of view, the evaluated $\langle\eta\rangle_{P_j}$ are summed with different weights as a function of the output power ($P_j$) in relation to the nominal one ($P_{\text{Nom}}$), this index being normalized by the summation of the weights. The normalized average efficiency rank index ($\langle\eta_{\text{rank}}\rangle$) is then numerically determined by (23), which corresponds to a dimensionless value for each filter, closely related to its efficiency. As can be noted, this step does not exclude any filter from the possible solution; instead, it allows to sort the filters by $\langle\eta_{\text{rank}}\rangle$

$$\langle\eta_{\text{rank}}\rangle = \frac{\sum_{P_1}^{P_j}\left[\left(\frac{1}{k}\sum_{C_1}^{C_k}\eta_{CkPj}\right)\frac{P_j}{P_{\text{Nom}}}\right]}{\sum_{P_1}^{P_j}\left[\frac{P_j}{P_{\text{Nom}}}\right]}. \tag{23}$$

*3) ZVS Constraint:* This step evaluates the ZVS condition, which is a mandatory constraint to be accomplished over whole converter operating range. Therefore, if one LLC filter from the set does not fill this requirement, it should be excluded from the possible solutions. Fig. 8 shows the HB main waveforms employed to analyze the true ZVS condition on the LLC converter. Here, $t_{\text{dis}}$ corresponds to the time required to deplete equivalent drain-to-source capacitance $C_{\text{DS}}$; $t_{\text{dead}}$ is the HB gate-driver dead time; and $t_{D\text{win}}$ is the duty-cycle window time, which is the maximum dead time that can be employed to achieve ZVS considering that $t_{\text{dead}} \geq t_{\text{dis}}$.

Mathematically, the true ZVS is achieved if the condition in (24a) and (24b) are true, which correspond to a system with inductive characteristic and enough dead time to discharge $C_{\text{DS}}$. With good accuracy, $t_{\text{dis}}$ can be estimated by (24c), which can be rewritten by (24d) in order to express the minimum tank current necessary at the end of the first half-cycle ($i_{S1.\text{off}}$) to deplete $C_{\text{DS}}$ within $t_{\text{dead}}$ interval

$$t_{\text{dis}} \leq t_{\text{dead}} \leq t_{D\text{win}} \tag{24a}$$

$$i_{S1.\text{on}} = i_{S1}(t_0) \leq 0 \tag{24b}$$

$$t_{\text{dis}} = \frac{2V_{\text{IN}}C_{\text{DS}}}{i_{S1.\text{off}}} \tag{24c}$$

$$i_{S1.\text{off}} \geq \frac{2V_{\text{IN}}C_{\text{DS}}}{t_{\text{dead}}} = i_{S1.\text{off.min}}. \tag{24d}$$

At this point, it is worth to mention that the TD procedure employed under the analysis discloses exact current level at the switching instant, which is not achieved by the FHA. Therefore, a trustful and reliable design is going to be accomplished.

*4) Switching Frequency Operating Range:* As a function of the LLC filter elements, the converter will need a different switching frequency range ($\Delta f_S$) in order to supply the load from the minimum to nominal output power covering all operating cases. Since the ZVS condition is evaluated in the last step, the remaining critical condition is related to the admissible maximum switching frequency ($f_{\text{ad.sw.max}}$), which is limited by the employed gate-driver circuit, usually a dedicated integrated circuit. Therefore, if a specific filter requires a $f_S$ higher than $f_{\text{ad.sw.max}}$ or wide $\Delta f_S$ (for instance, $>f_o/2$), it will be excluded from the possible solutions.

*5) Power Density Evaluation:* The proposed design procedure does not aim to optimize the converter power density; however, to give the designer a view of the power density among the resonant tank set, the volume of magnetic elements is available to be assessed before the final filter selection. Furthermore, as

TABLE II
LED DRIVER SPECIFICATION

| Application Parameters | Designator | Min | Max |
|---|---|---|---|
| Half-bridge input voltage | $V_{IN}$ | 320 $V$ | 420 $V$ |
| Average output current | $I_O$ | 0.25 $A$ | 1.15 $A$ |
| Outcome power | $P_O$ | 20 $W$ | 100 $W$ |
| Outcome output voltage | $V_O$ | 81.17 $V$ | 87.37 $V$ |
| Resonant switching frequency | $f_o$ | 100 $kHz$ | |
| LED module forward voltage drop | $V_{th}$ | 80.22 $V$ | |
| LED module series resistance | $r_{ac}$ | 6.22 Ω | |

TABLE III
LLC COMPONENT COMPARISON BETWEEN THE CLASSICAL FHA AND PROPOSED DESIGN PROCEDURE

| Parameter | Value | |
|---|---|---|
| | FHA ($F_{12}$) | Proposed ($F_4$) |
| Resonant capacitor ($C_S$) | 12 nF | 6.8 nF |
| Resonant inductance ($L_S$) | 211 $\mu$H | 372 $\mu$H |
| Resonant inductor EE core | EE 25/10/06 | EE 25/10/06 |
| Magnetizing inductance ($L_M$) | 633 $\mu$H | 1117 $\mu$H |
| Transformer turns ratio ($n$) | 2.28 | 2.28 |
| Transformer EE core | EE 30/15/14 | EE 30/15/14 |
| Output capacitor ($C_O$) | 10 $\mu$F/100V | 10 $\mu$F/100V |
| Gate-driver dead-time ($t_{dead}$) | 350 $ns$ | 450 $ns$ |
| HB MOSFET ($S_1$, $S_2$) | IPP50R280CE | IPP50R280CE |
| Rectifier diodes ($D_1$, $D_2$) | SB3200TA | SB3200TA |

a function of the rms voltage in $C_S$, the capacitor volume also changes, deteriorating the system power density if extra large $v_{Cs.\text{rms}}$ is noticed.

*6) Final LLC Component Selection:* In order to support the final filter selection and avoid a laborious data analysis, Step 5 main information are condensed in a table, which presents the filters sorted by the $\langle \eta_{\text{rank}} \rangle$, together with the ZVS condition (YES or NOT), minimum, maximum, and switching frequency range, maximum $t_{\text{dis}}$, transformer and inductor magnetic core size, and maximum $C_S$ rms voltage.

## VI. DESIGN EXAMPLE: LLC LED DRIVER

Employing the proposed design procedure, the LLC converter is designed to supply an LED-based load. Table II presents the application specifications. As can be seen, the LLC converter has to present the capability to supply the LED with different current levels considering a wide $V_{\text{IN}}$ variation.

Carefully following the proposed design procedure, from the initial set given by 24 filters ($F_1, F_2, ..., F_{24}$), the filter $F_4$ specified in Table III has been selected. With the purpose of developing a comparative analysis, Table III also presents the parameters of the LLC LED driver obtained, following the classical design procedure based on FHA. The resonant tank elements defined by the classical procedure correspond to filter $F_{12}$ of the set evaluated in the proposed design.

In order to elucidate the proposed and the classical design procedures, supplementary material attached to this manuscript presents in detail the step-by-step development of each design methodology. To implement these design procedure algorithms, the Wolfram MATHEMATICA v.12 software is employed.

Nevertheless, for the sake of clarity, only the last step of the proposed design procedure is detailed here. Therefore, considering the application specifications presented in Table II and the set of 24 filters detailed in the supplementary material, the support data table from the last step of the proposed procedure is presented in Table IV. As can be seen, the filters $F_i$ are sorted by the $\langle \eta_{\text{rank}} \rangle$ index, which is closely related to the converter average efficiency, and for each filter, their main performance parameters are presented to support the selection of the most prominent filter. Analyzing the data in Table IV, filters $F_8$, $F_7$, and $F_6$ are not selected due to the absence of ZVS over the whole operating range. Filters $F_{16}$, $F_{15}$, $F_{24}$, $F_{14}$, $F_{23}$, and $F_{22}$ are avoided here due to the required switching frequency range $\Delta f_S$, that is higher than 50 kHz. Filter $F_5$ is not selected due to the small difference between $t_{D\text{win}}$ and $t_{\text{dis}}$, which can lead to the loss of ZVS due to the component tolerance and parasitic elements that are neglected in the analysis. So, filter $F_4$ is selected as the result of the proposed design procedure since it has the highest $\langle \eta_{\text{rank}} \rangle$ index and does not violate other constraints.

Comparing $F_4$ and $F_{12}$, it can be seen that both filters present ZVS, have similar $\Delta f_S$, employ the same magnetic core size, and have very close $\langle \eta_{\text{rank}} \rangle$ index.

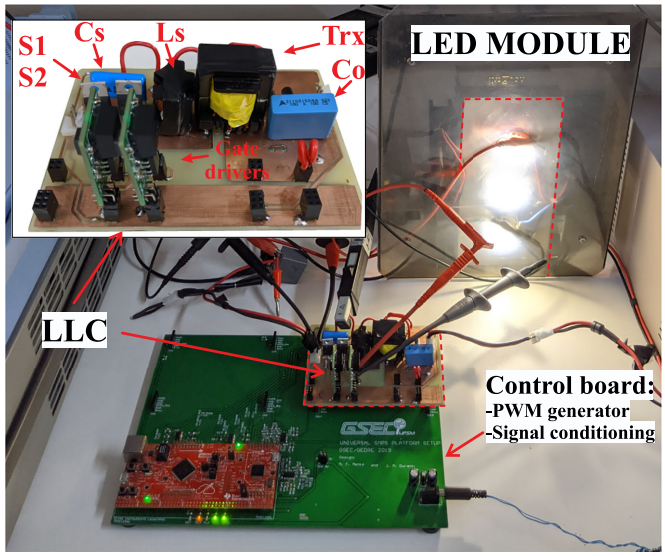


Fig. 9. $F_4$ LLC LED driver experimental setup.

## VII. EXPERIMENTAL RESULTS

Experimental results are presented in this section with two purposes: 1) show the feasibility of the TD analysis and predict accurately the LLC LED driver operation; and 2) evaluate the real performance of the designed LLC LED driver, assessing the converter efficiency, switching frequency range, and ZVS condition. Fig. 9 shows experimental prototype of the LLC LED driver design following the proposed procedure.

### A. TD-Based Analysis of the LLC LED Driver

This section follows employing the proposed TD analysis described in Sections III and IV, and considering the parameters of the LLC filter $F_4$.

TABLE IV
FINAL LLC FILTER SELECTION SUPPORT DATA

| $F_i$ | $\eta_{rank}$ | $Min[t_{Dwin} - t_{dis}]$ C1 | C2 | ZVS | $Max[t_{dis}]$ $(ns)$ | $f_{S.MIN}$ $(kHz)$ | $f_{S.MAX}$ $(kHz)$ | $\Delta f_S$ $(kHz)$ | Transformer Core | $L_S$ Core | Max$[V_{Cs}]$ |
|---|---|---|---|---|---|---|---|---|---|---|---|
| 8 | 0.969647 | -394.466 | 299.695 | **NO** | 648.912 | 70.9582 | 131.516 | 60.5574 | EE.30/15/14 | EE.25/10/6 | 287.659 |
| 7 | 0.968685 | -241.108 | 353.905 | **NO** | 550.24 | 73.0721 | 128.361 | 55.2886 | EE.30/15/14 | EE.25/10/6 | 281.122 |
| 16 | 0.967982 | 417.518 | 640.447 | YES | 385.534 | 71.6354 | 136.81 | **65.1747** | EE.30/15/14 | EE.20/10/5 | 224.107 |
| 6 | 0.967486 | -87.9653 | 420.912 | **NO** | 490.147 | 75.3211 | 125.094 | 49.7733 | EE.30/15/14 | EE.25/10/6 | 275.245 |
| 15 | 0.966515 | 538.103 | 719.13 | YES | 353.156 | 73.7291 | 132.321 | **58.5922** | EE.30/15/14 | EE.20/10/5 | 225.121 |
| 24 | 0.966002 | 731.265 | 797.812 | YES | 327.48 | 71.9969 | 138.719 | **66.7225** | EE.30/15/14 | EE.20/10/5 | 220.262 |
| 5 | 0.965957 | **72.832** | 505.185 | YES | 444.332 | 77.7176 | 121.748 | 44.0302 | EE.30/15/14 | EE.25/10/6 | 270.326 |
| 14 | 0.964687 | 674.432 | 812.236 | YES | 319.908 | 75.9489 | 128.103 | **52.1543** | EE.30/15/14 | EE.20/10/5 | 226.495 |
| 23 | 0.964483 | 856.286 | 883.649 | YES | 298.519 | 74.0728 | 133.893 | **59.8202** | EE.30/15/14 | EE.20/10/5 | 221.229 |
| 4 | 0.963943 | 250.643 | 613.183 | YES | 393.594 | 80.276 | 118.412 | 38.1357 | EE.30/15/14 | EE.25/10/6 | 266.894 |
| 22 | 0.962326 | 995.221 | 983.1 | YES | 269.32 | 76.2695 | 129.425 | **53.1557** | EE.30/15/14 | EE.20/10/5 | 222.555 |
| 13 | 0.961177 | 829.847 | 923.16 | YES | 285.905 | 78.3055 | 124.167 | 45.8615 | EE.30/15/14 | EE.25/10/6 | 228.445 |
| 3 | 0.961168 | 457.849 | 754.33 | YES | 340.112 | 83.0119 | 115.261 | 32.2494 | EE.30/15/14 | EE.25/10/6 | 265.989 |
| 12 | 0.957984 | 1007.71 | 1056.01 | YES | 250.911 | 80.8113 | 120.481 | 39.6692 | EE.30/15/14 | EE.25/10/6 | 231.374 |

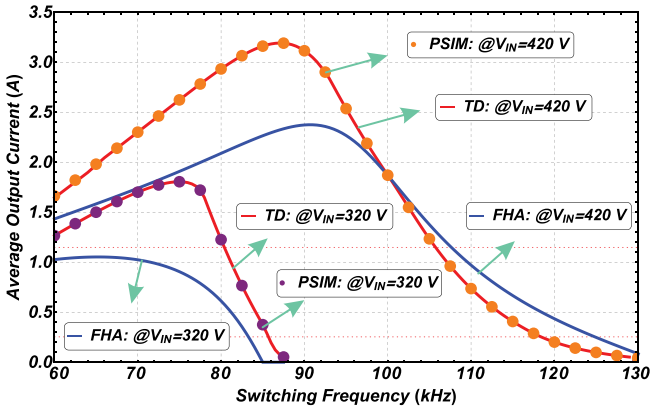


Fig. 10. LLC filter $F_4$ LED driver current gain curve.

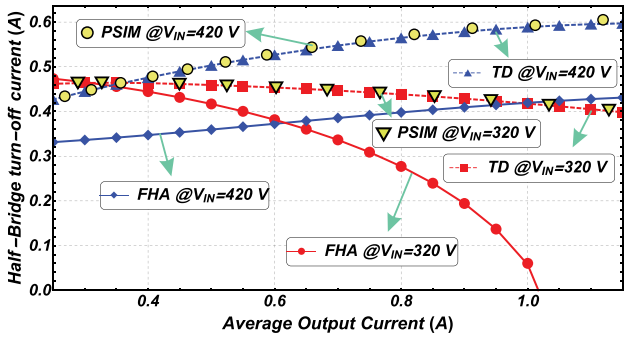


Fig. 11. Half-bridge switches turn-OFF current prediction with TD and FHA approaches in comparison to PSIM simulation results.

*1) Current Gain Curve:* In order to evaluate the current gain curve of the designed converter, Fig. 10 shows the LED current as a function of the inverter $f_S$. These curves are obtained employing the proposed TD analysis, classical FHA approach, and PSIM simulation results for the LED driver operating with $V_{\text{IN}} = 320$ V and $V_{\text{IN}} = 420$ V. Since the LLC is considered ideal under TD and FHA analyses, the same idealized conditions are employed in PSIM to outcome a fair comparison. Presuming PSIM results as the converter real behavior, it is clearly noted in Fig. 10 that the proposed TD analysis accurately predicts the LED current regardless of operating $f_S$. On the other hand, results from FHA approach present considerable deviation when $f_S$ moves away from main resonance $f_o$. The inaccuracy of the FHA approach reflects on the predicted $f_S$ range, maximum peak gain, and consequently upon current and voltage levels throughout the converter, which are key parameters that have to be known to enhance the LLC performance.

*2) HB and Resonant Tank Current Prediction:* To achieve an enhanced LLC analysis that supports the design toward improved performance, among other parameters, it is essential to accurately predict the HB switches and resonant tank current levels. Fig. 11 shows the predicted HB switches turn-OFF($i_{S1.\text{off}}$) current employing the FHA and TD approaches in comparison to PSIM results. As can be seen, presuming PSIM results as the accurate one, TD-based analysis presents an outstanding level of accuracy compared to FHA approach results. In addition, to support this statement, Fig. 12 shows the percentage error of the FHA in predicting HB $i_{S1.\text{off}}$ and rms current ($i_{S1.\text{rms}}$) as well as LLC resonant rms ($i_{R.\text{rms}}$) and peak ($i_{R.\text{PK}}$) current values under different input voltages. As can be seen, with the expense of an error up to 10%, FHA approach could be employed only to predict the HB rms current and filter rms current for $V_{\text{IN}} = 320$ V. Nevertheless, in a general way, seeking for results with high accuracy, it can be concluded that FHA analysis is not reliable.

Since the proposed TD analysis accurately predicts the LLC current levels, it can be employed to perform several analysis. To highlight this feature, Fig. 13 compares $i_{S1.\text{off}}$ and $i_{R.\text{rms}}$ current levels for the LLC designed by the proposed and classical procedures. From this analysis, it can be seen that the proposed design outcomes in an LLC with reduced currents, which is expected to enhance, for instance, the converter efficiency.

*3) Time-Domain Waveform:* Besides the quantified current levels evaluation, a powerful tool corresponds to waveform assessment, which provides further insights of the converter, revealing its operation mode as well as switches and diodes commutation characteristics [ZVS and zero current switching (ZCS)]. In this context, Fig. 14 shows main current waveforms of the LLC LED driver predicted employing TD and FHA analyses in comparison to PSIM simulation results. As can be seen, considering the extreme input voltage and load conditions, the TD predicted waveform is exactly the same as the one given by PSIM simulations.

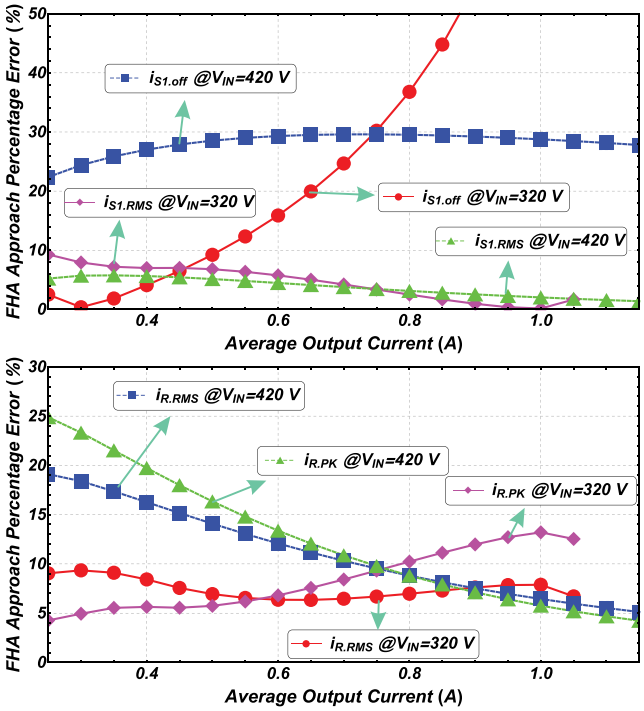


Fig. 12. FHA approach percentage error in predicting LLC converter currents.

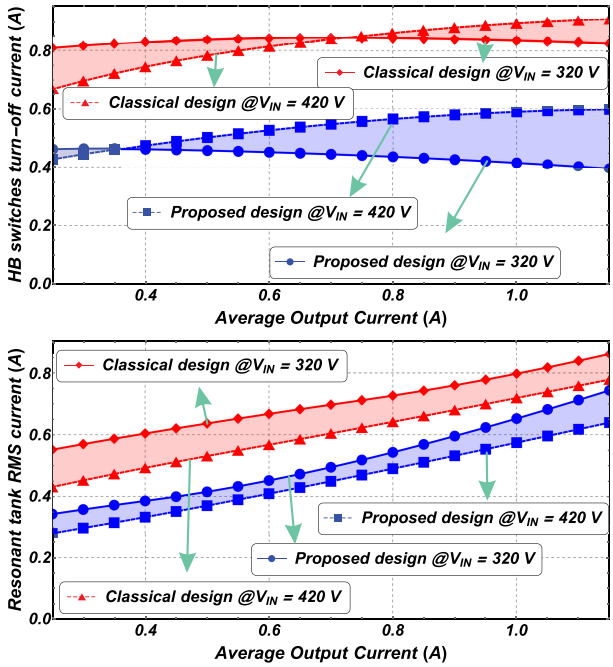


Fig. 13. Classical and proposed design current level comparison employing TD analysis.

To show the feasibility of the predicted waveform and TD analysis, experimental waveforms for the same operating points are shown in Fig. 15. As it can be seen, the predicted converter waveforms employing the TD procedure are analogous to the experimentally measured. Further assessing Fig. 15, it should be noted that due to the neglected parasitic components,

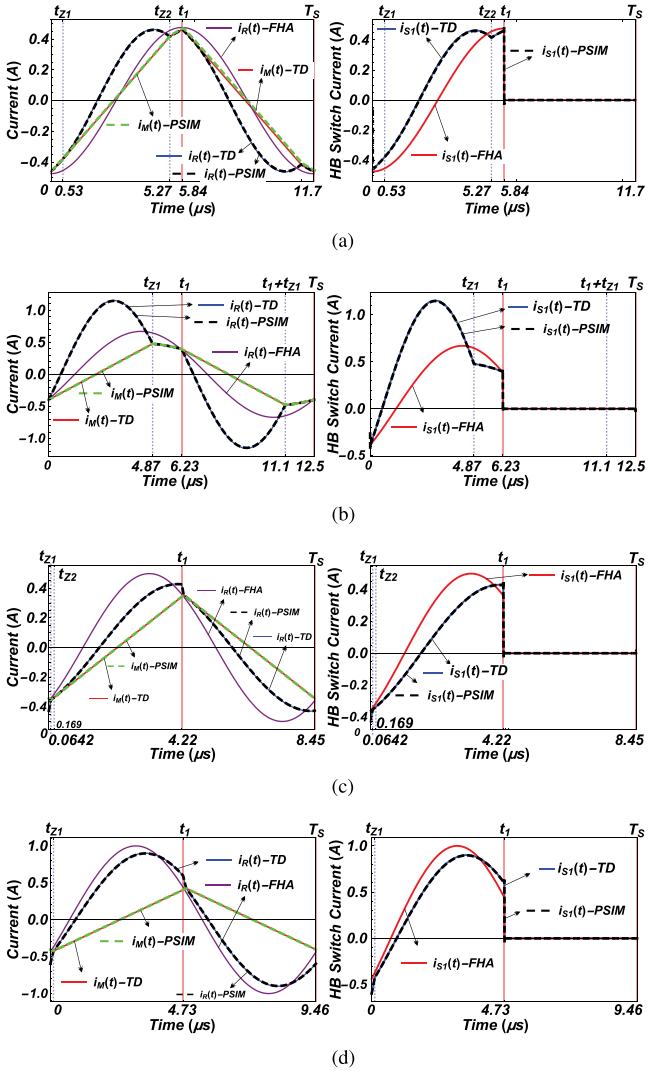


Fig. 14. Predicted time-domain behavior of the converter employing the proposed procedure in comparison to FHA and PSIM simulation results. (a) $V_{IN}$ = 320 V , $I_O$ = 0.25 A and $f_S$ = 85656 Hz. OPO mode. (b) $V_{IN}$ = 320 V , $I_O$ = 1.15 A and $f_S$ = 80276 Hz. PO mode. (c) $V_{IN}$ = 420 V , $I_O$ = 0.25 A and $f_S$ = 118412 Hz. NOP mode. (d) $V_{IN}$ = 320 V , $I_O$ = 1.15 A and $f_S$ = 105656 Hz. NP mode.

experimentally, the $f_S$ has to be adjusted in order to achieve the desired average output current. Furthermore, for the same reason, some waveforms diverge from the theoretically analyzed (see Fig. 4), that is the case for the secondary side rectified current ($|ni_P| = n|i_R - i_M|$), which make it impossible to precisely define the transition time on the experimental results for $V_{\text{IN}} = 420$ V. The assumption that all the elements are ideal corresponds to the main limitation of the proposed TD analysis, where solution is out of the scope of this work.

In addition to the waveform plot, the converter operation mode for each specific operating condition is easily assessed by extracting this information from the $C_kF_i$.csv files. In this way, Table V presents the predicted operation mode and required $f_S$ to obtain the specific output current for the different $V_{\text{IN}}$. As can be seen, PO and OPO modes are noted when $V_{\text{IN}} = 320$ V, which implies in ZCS for the output rectifier. On the other hand, for

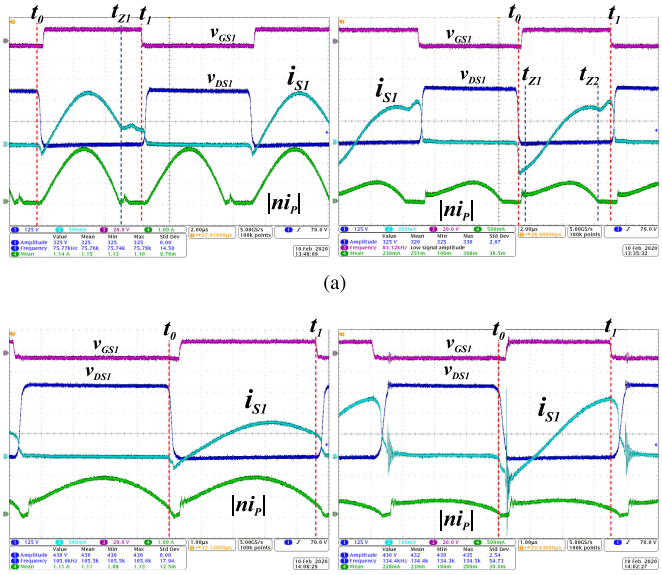


Fig. 15. LLC LED driver experimental main waveforms at extreme operating point.(a) $V_{IN} = 320$ V; Left side: $I_O = 1.15$ A and $f_S \approx 76$ KHz; Right side: $I_O = 0.25$ A and $f_S \approx 83$ KHz. (b) $V_{IN} = 420$ V; Left side: $I_O = 1.15$ A and $f_S \approx 106$ KHz; Right side: $I_O = 0.25$ A and $f_S \approx 134$ KHz.

TABLE V
FILTER $F_4$ PREDICTED $f_S$ AND OPERATION MODES

| | $V_{BUS} = 320\ V$ | | $V_{BUS} = 420\ V$ | |
|---|---|---|---|---|
| $I_O$ | Mode | $f_S$ | Mode | $f_S$ |
| 0.25 | OPO | 85656 | NOP | 118412 |
| 0.35 | OPO | 85107 | NP | 116068 |
| 0.45 | PO | 84442 | NP | 114147 |
| 0.55 | PO | 83771 | NP | 112497 |
| 0.65 | PO | 83131 | NP | 111052 |
| 0.75 | PO | 82518 | NP | 109766 |
| 0.80 | PO | 82220 | NP | 109172 |
| 0.95 | PO | 81359 | NP | 107547 |
| 1.15 | PO | 80276 | NP | 105656 |

the maximum input voltage $V_{\text{IN}} = 420$ V, NP mode is noted over almost the whole range. NP mode occurs when the converter is operated above the main resonance, condition where ZCS is lost on the secondary side.

At this point, it is worth to mention that simulation softwares like PSIM are accepted to be very accurate and can be easily employed to get the converter waveform. However, to obtain this result, it is required to numerically solve the ODE with a given initial condition from period to period and update the initial conditions at the beginning of each period until they reach the steady-state condition, which demands cumbersome numerical methods and are inconvenient once usually the main interest is the steady-state operation. In contrast, the proposed TD procedure relies on the steady-state operation outcoming in results as accurate as PSIM without the expense of transient period computation. Furthermore, once the converter is solved in a mathematical environment, several analyses can be developed, going from the exhaustive converter analysis to optimized designed converter design procedure.

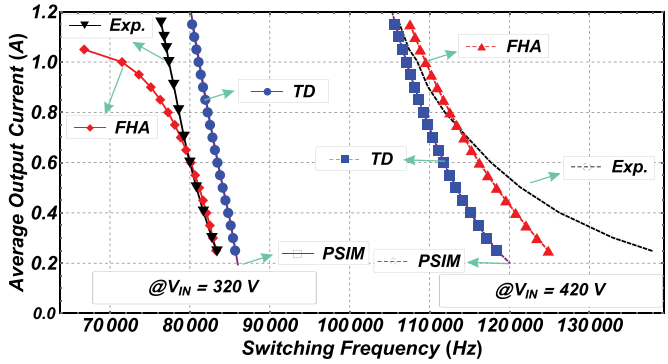


Fig. 16. Switching frequency range analysis of the LLC LED driver designed by the proposed procedure, filter $F_4$.

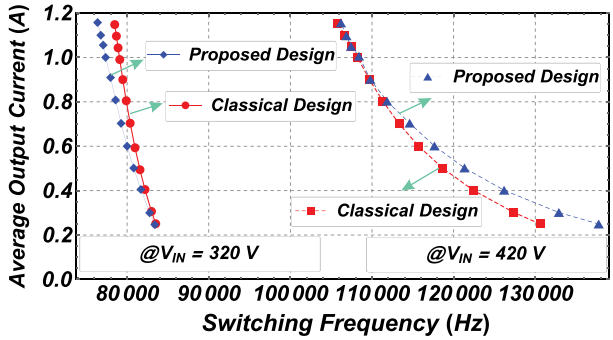


Fig. 17. Proposed and classical design experimental switching frequency range comparison.

### B. Performance Evaluation of LLC LED Driver

Since the proposed TD analysis feasibility has been evaluated, this section deals with the required analysis to validate the feasibility of the proposed design procedure.

*1) Switching Frequency Range:* The switching frequency range required by $F_4$ to maintain the output current controlled over the wide input voltage range and load variation is shown in Fig. 16, where PSIM and experimental results are presented in comparison to the prediction by FHA and proposed TD procedure. As it can be seen, TD and PSIM results are interchangeable. In addition, comparing experimental (Exp.) and TD results for $V_{\text{BUS}} = 320$ V, there is a difference between the results given by an almost constant value, which shift the curves. However, both experimental and TD curves present the same inclination, which cannot be observed in the results predicted by the FHA approach. On the other hand, for $V_{\text{BUS}} = 420$ V, the experimental switching frequency curve has its shape deviated from the predicted one by TD and FHA analyses. These errors between experimental and TD-based results are given by parasitic components, neglected in the TD analysis, as well as element tolerance. Fig. 17 compares the switching frequency range between classical and proposed designs. As expected and predicted by the TD analysis, both designs present a similar range.

*2) ZVS Constraint Evaluation:* To achieve true ZVS, it is mandatory to address the constraints given in (24), which states that $t_{\text{dis}} \leq t_{\text{dead}} \leq t_{D\text{win}}$ and $i_{S1.\text{on}} = i_{S1}(t_0) \leq 0$. Therefore, in

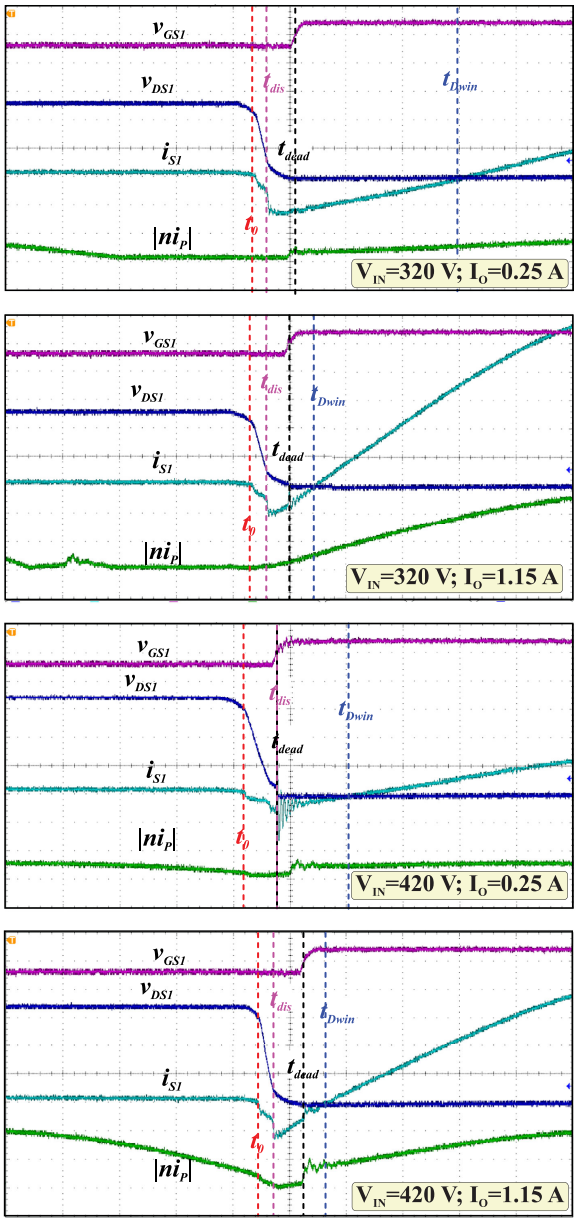


Fig. 18. ZVS analysis of the LLC LED driver designed by the proposed procedure, filter $F_4$.

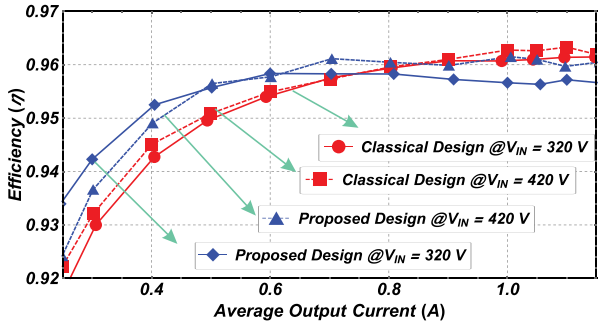


Fig. 19. Experimental efficiency comparison between classical and proposed LLC LED driver designs.

order to evaluate this condition experimentally, Fig. 18 shows HB inverter main waveform during the switches turn-ON process for the extreme operation conditions, going from $V_{\rm IN} = 320$ V with $I_O = 1.15$ A to $V_{\rm IN} = 420$ V with $I_O = 0.25$ A. Analyzing these waveforms, it can be seen that $i_{S1}(t_0) \leq 0$ for these operating points. In addition, except for $V_{\rm IN} = 420$ V with $I_O = 0.25$ A, it can be noted that $t_{\rm dis} \leq t_{\rm dead} \leq t_{D\rm win}$ assuring in this way ZVS to the HB switches. On the other hand, for $V_{\rm IN} = 420$ V with $I_O = 0.25$ A, it can be noted that $S_1$ is turned ON before completely depleting $C_{\rm DS}$, loosing, therefore, ZVS condition. It was later detected that a safe conservative margin is required especially under (24) evaluation during the final filter selection. There are several issues that affect this condition which are important to bear in mind; for instance, $C_{\rm DS}$ are nonlinear capacitors and their value is a function of the drain-to-source voltage. Furthermore, at the resonant tank input point, the total capacitance is the sum of the output MOSFET capacitors $C_{\rm DS}$ and the parasitic capacitance $C$stray of the power MOSFET cases, the heat sink, the intrawinding capacitance of the resonant inductor, etc. On the other hand, MOSFETs and gate-driver turn-OFF and turn-ON delay also impact in this constraint assessment. Furthermore, the error in predicting the correct $f_S$ for operation above $f_o$, which is mainly associated with transformer intrawinding capacitance, also impairs the accuracy in predicting the correct ZVS condition range. These issues related to parasitic components once more highlight the main limitation of the proposed TD procedure.

*3) Efficiency Curve Evaluation:* Finally, Fig. 19 shows the experimental efficiency of the classical and proposed designs for the extreme $V_{\rm IN}$ as a function of the LED load current. As can be seen, both designs present high efficiency over the whole operating range. In addition, comparing both designs, it can be noted that the proposed design presents higher efficiency than the classical design when the output power is reduced. Nevertheless, around nominal power, the proposed design presents a deteriorated efficiency. For the proposed design, employing experimental results, its computed $\langle \eta_{\rm rank} \rangle = 0.9569$. In the same way, for the classical design, this computation results in $\langle \eta_{\rm rank} \rangle = 0.9565$. Compared to the theoretical $\langle \eta_{\rm rank} \rangle$, the error is less than 1%. At this point, it should be noted that the proposed design does not aim to achieve an optimal solution since optimization tools are not employed. In spite of this, the proposed design, besides the own filter design, allows to accurately predict, during the design stage, the performance of the converter. So, based on the design requirements, it is possible to adjust the design even before experimental development. To support this statement, Fig. 20 shows the predicted efficiency of both designs employing the proposed design procedure, which is very close to the measured experimental efficiency.

Additionally, a slight divergence ($\approx 1.5\%$) between theoretical and experimental efficiency for the proposed design when operating around the nominal power should be noted. This discrepancy can be assigned to the neglected parasitic components since an operating condition different from the real one is predicted due to the idealized analysis, which also influences the loss computation and consequently the estimated efficiency.

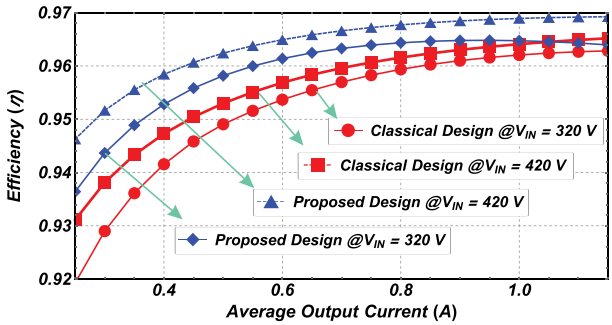


Fig. 20. Theoretical efficiency comparison between classical and proposed LLC LED driver designs.

### C. Final Remarks

At this point, since the LLC LED driver converter is designed, its control system can be developed. Usually, implementing PFM, the control system changes the inverter $f_S$ to maintain output LED current-controlled. Further details of the LLC LED driver control system are presented in [19]. Regarding the proposed TD analysis, which is claimed to be one of the main contributions of this article, an enhanced accuracy in comparison to the FHA approach is noticeable. In addition, since the LED PWL circuit was considered under the LLC TD analysis, it outcomes in a more general solution, which can be directly applied to analyze the LLC for a battery charger as well as further applications where the load is purely resistive. The proposed design procedure, also claimed as one contribution, outcomes in a well-designed LLC LED driver, maintaining high efficiency over a wide operating range, enough current gain, and ensuring soft switching with ZVS condition. Nevertheless, even developing several analyses to outcome with the filter components, care must be taken to not stamp this procedure as an optimized design methodology since optimization algorithms have not been employed. In addition, the merit of the proposed design in accurately predicting numerous performance indicators should be recognized, for instance, converter current levels, switching frequency range, power density, and average efficiency.

Finally, it is worth to mention that even by achieving enhanced results in both TD analysis and design procedure, the main limitation of this study is related to the filter parasitic elements, which are neglected throughout the analysis, impairing the accuracy in a general way.

## VIII. CONCLUSION

This article presented a high accurate TD analysis and a new design procedure for the LLC LED driver. The TD analysis is accomplished throughout the system state-space representation direct TD solution. In comparison to the FHA approach, outstanding accuracy is achieved by employing the proposed TD solution procedure. Experimental and simulation results show the feasibility of the proposed TD analysis procedure. With the LLC LED driver faithfully solved on the TD, a new design procedure is proposed. Similar to previous design procedure, the design was guided by the estimated efficiency of the LLC LED driver operating over a wide range. To take into account the efficiency of the converter under different operating cases and load, a figure of merit based on the weighted average efficiency was introduced. This index serves to sort the set of considered resonant filters. Together with the average efficiency rank, additional constraints are assessed before selecting the resonant filter. This constraint ensures to the system enough current gain and ZVS over the whole system operating window.

## REFERENCES

[1] R. Yu, G. K. Y. Ho, B. M. H. Pong, B. W.-K. Ling, and J. Lam, "Computer-aided design and optimization of high-efficiency LLC series resonant converter," *IEEE Trans. Power Electron.*, vol. 27, no. 7, pp. 3243–3256, Jul. 2012.

[2] S. D. Simone, C. Adragna, C. Spini, and G. Gattavari, "Design-oriented steady-state analysis of LLC resonant converters based on FHA," in *Proc. Int. Symp. Power Electron. Electrical Drives Autom. Motion SPEEDAM 2006*, 2006, pp. 200–207.

[3] N. Shafiei, M. A. Saket, and M. Ordonez, "Time domain analysis of LLC resonant converters in the boost mode for battery charger applications," in *Proc. IEEE Energy Convers. Congr. Expo.*, 2017, pp. 4157–4162.

[4] C. A. Cheng, C. H. Chang, T. Y. Chung, and F. L. Yang, "Design and implementation of a single-stage driver for supplying an LED street-lighting module with power factor corrections," *IEEE Trans. Power Electron.*, vol. 30, no. 2, pp. 956–966, Feb. 2015.

[5] W. Feng, F. C. Lee, and P. Mattavelli, "Optimal trajectory control of LLC resonant converters for LED PWM dimming," *IEEE Trans. Power Electron.*, vol. 29, no. 2, pp. 979–987, Feb. 2014.

[6] H. Wu, "Multi-channel constant current (MC3) LED driver for indoor LED luminaries," M.S. thesis, Faculty Virginia Polytechnic Institute, 2011.

[7] Q. Zhang *et al.*, "A center point iteration MPPT method with application on the frequency-modulated LLC microinverter," *IEEE Trans. Power Electron.*, vol. 29, no. 3, pp. 1262–1274, Mar. 2014.

[8] R. Steigerwald, "A comparison of half-bridge resonant converter topologies," *IEEE Trans. Power Electron.*, vol. 3, no. 2, pp. 174–182, Apr. 1988.

[9] X. Fang, H. Hu, Z. J. Shen, and I. Batarseh, "Operation mode analysis and peak gain approximation of the LLC resonant converter," *IEEE Trans. Power Electron.*, vol. 27, no. 4, pp. 1985–1995, Apr. 2012.

[10] J. Deng, C. C. Mi, R. Ma, and S. Li, "Design of LLC resonant converters based on operation-mode analysis for level two PHEV battery chargers," *IEEE/ASME Trans. Mechatronics*, vol. 20, no. 4, pp. 1595–1606, Sep. 2015.

[11] J. F. Lazar and R. Martinelli, "Steady-state analysis of the LLC series resonant converter," in *Proc. 16th Annu. IEEE Appl. Power Electron. Conf. Expo. APEC 2001*, vol. 2, 2001, pp. 728–735.

[12] H. Wang, S. Dusmez, and A. Khaligh, "Maximum efficiency point tracking technique for LLC-based PEV chargers through variable DC link control," *IEEE Trans. Ind. Electron.*, vol. 61, no. 11, pp. 6041–6049, Nov. 2014.

[13] Z. Fang, T. Cai, S. Duan, and C. Chen, "Optimal design methodology for LLC resonant converter in battery charging applications based on time-weighted average efficiency," *IEEE Trans. Power Electron.*, vol. 30, no. 10, pp. 5469–5483, Oct. 2015.

[14] U. Mumtahina and P. J. Wolfs, "Multimode optimization of the phase-shifted LLC series resonant converter," *IEEE Trans. Power Electron.*, vol. 33, no. 12, pp. 10 478–10 489, Dec. 2018.

[15] M. Daryaei, M. Ebrahimi, and S. A. Khajehoddin, "Alternative approach to analysis and design of series resonant converter at steady state," *IEEE Trans. Ind. Electron.*, vol. 66, no. 6, pp. 4424–4435, Jun. 2019.

[16] M. P. Foster, H. I. Sewell, C. M. Bingham, D. A. Stone, D. Hente, and D. Howe, "Cyclic-averaging for high-speed analysis of resonant converters," *IEEE Trans. Power Electron.*, vol. 18, no. 4, pp. 985–993, Jul. 2003.

[17] C. T. Chen, *Analog and Digital Control System Design: Transfer-Function, State-Space, and Algebraic Methods*, 1st ed. Oxford, U.K.: Oxford University Press, 1995.

[18] C-T. Chen, *Linear System Theory and Design*, 4th ed. Oxford, U.K.: Oxford University Press, 2012.

[19] M. F. Menke, A. R. Seidel, and R. V. Tambara, "LLC LED driver small-signal modeling and digital control design for active ripple compensation," *IEEE Trans. Ind. Electron.*, vol. 66, no. 1, pp. 387–396, Jan. 2019.

**Maikel F. Menke** (Student Member, IEEE) was born in Três de Maio, Brazil, in 1989. He received the B.Sc. and M.Sc. degrees in electrical engineering from the Federal University of Santa Maria (UFSM), Santa Maria, Brazil, in 2015 and 2016, respectively. He is currently working toward the Ph.D. degree in electrical engineering with the Federal University of Santa Maria.

Since 2019, he has been a Professor with the Federal Institute of Santa Catarina (IFSC), Santa Catarina, Brazil. Also, he has been a Researcher with the GEDRE/UFSM Intelligence in Lighting research group since 2009, and with Electrical and Computational Systems Research and Development Group (GSEC) since 2010. His research interests include artificial lighting systems, LED drivers, power factor correction, resonant converters, self-oscillating systems, and control applied to LED drivers.

**João P. Duranti** was born in Palmeira das Missões, Brazil, in 2000. He is currently working toward the undergraduate degree in electrical engineering with the Federal University of Santa Maria (UFSM), Santa Maria, Brazil.

Since 2015, he has been a member of Electrical and Computational Systems Research and Development Group (GSEC), Santa Maria, Brazil. His research interests include dc–dc power converters, resonant converters, and LED drivers.

**Leandro Roggia** was born in Santa Maria, Brazil, in 1985. He received the B.S., M.S., and Ph.D. degrees in electrical engineering from the Federal University of Santa Maria, Santa Maria, Brazil, in 2008, 2010, and 2013, respectively.

From 2010 to 2013, he was a Professor with Federal Institute of Rio Grande do Sul, Brazil. Currently, he is with the Federal University of Santa Maria, where he is a Professor with the Technical Industrial School of Santa Maria. He has been a Researcher with Power Electronics and Control Group (GEPOC) since 2003, and with the Electrical and Computational Systems Research and Development Group (GSEC) since 2013. His research interests include power electronics, dc–dc converters, energy storage devices, converters for photovoltaic systems, LED drivers, and power factor correction.

Dr. Roggia is member of the Brazilian Power Electronics Society (SOBRAEP).

**Fábio E. Bisogno** was born in Santa Maria, Brazil, in 1973. He received the B.S. and M.Sc. degrees in electrical engineering from the Federal University of Santa Maria, Santa Maria, Brazil, in 1999 and 2001, respectively. He received the Dr.-Ing. degree in electrical engineering and information technology from the Chemnitz University of Technology, Chemnitz, Germany, in 2006.

From 2003 to 2009, he was a Researcher with the Fraunhofer Institute for Autonomous Intelligent Systems (AIS), with Intelligent Analysis and Information Systems (IAIS), and with Reliability and Microintegration (IZM), Germany. Currently, he is a Professor with Federal University of Santa Maria and develops research on power electronic with Electronic Power and Control Group (GEPOC) and Computational Systems Research and Development Group (GSEC). His research interests include resonant converters, lighting systems, self-oscillating systems, piezoelectric transformers, and uninterruptible power supplies.

**Rodrigo V. Tambara** was born in Santa Maria, Brazil, in 1987. He received the B.S., M.Sc., and Ph.D. degrees in electrical engineering from the Federal University of Santa Maria, Santa Maria, Brazil, in 2008, 2010, and 2014, respectively.

From 2014 to 2016, he was an Adjunct Professor with the Universidade Franciscana, Santa Maria, Brazil. From 2016 to 2018, he was an Adjunct Professor with the Federal University of Santa Maria, Cachoeira do Sul, Brazil. Currently, he is with the Federal University of Santa Maria, where he is a Adjunct Professor with the Colégio Técnico Industrial de Santa Maria. He has been a Researcher with Power Electronics and Control Group (GEPOC) since 2004, and with the Electrical and Computational Systems Research and Development Group (GSEC) since 2015. His research interests include adaptive control, grid-connected converters, dimming systems, and LED drivers.

Dr. Tambara is a member of the Brazilian Power Electronics Society and also a member of the Brazilian Automatic Control Society. He is a reviewer for the *Brazilian Power Electronics Society*, *Brazilian Automatic Control Society*, and IET magazines.

**Álysson R. Seidel** (Member, IEEE) was born in São Pedro do Sul, Brazil, in 1975. He received the B.S. and Ph.D. degrees in electrical engineering from the Federal University of Santa Maria, Santa Maria, Brazil, in 1999 and 2004, respectively.

From 2004 to 2008, he was an Associate Professor with the Department of Electrical Engineering, University of Passo Fundo, Passo Fundo, Brazil. Currently, he is with Federal University of Santa Maria, where he is a Professor with the Technical Industrial School of Santa Maria. He has been a Researcher with Electronic Ballast Research Group (GEDRE) since 1997, and with the Electrical and Computational Systems Research and Development Group (GSEC) since 2010. His research interests include resonant converters, dimming systems, simulation, discharge lamps, and lighting systems.